Using a Streak Camera to Resolve the Motion of Molecular Excited States with Picosecond Time Resolution and 150 nm Spatial Resolution

Astrid M. Müller and Christopher J. Bardeen*

Department of Chemistry, University of California, Riverside, California 92521

Received: April 13, 2007; In Final Form: June 7, 2007

A one-dimensional streak camera imaging (1D-SCI) experiment to visualize the spatial motion of luminescent excited-state species in condensed phase systems is presented. A femtosecond pulse is focused through an objective lens to create a localized excited-state population, using either one-photon or two-photon excitation conditions. The time-dependent emission from this spot is then imaged onto the horizontal entrance slit of a streak camera. The resulting one-dimensional projection of the emission spot is detected with picosecond time resolution. Using this setup, the ability to resolve broadening of the excitation spot due to diffusive motion on the order of 150 nm is demonstrated. The 1D-SCI technique is successfully employed to image the translational diffusion of excited-state platinum octaethylporphyrin molecules in a toluene solution at various concentrations. In addition, the absence of long-range ($>1\ \mu$m) electronic energy transfer in the polymer polyvinylcarbazole is confirmed. In both of these samples, the absorption and emission spectra are well-separated, and the luminescence can escape the sample without reabsorption playing a role. Preliminary experiments on disodium fluorescein, a molecule with a small fluorescence Stokes shift, exhibit anomalously rapid broadening. This is most likely due to fluorescence reabsorption and re-emission, although the simplest model of nonradiative transport fails to capture the observed behavior. In principle, changes in the optical arrangement could improve the spatial resolution of this experiment to approximately 60 nm, given the current experimental signal-to-noise ratio. Other potential improvements and limitations of the technique are also discussed.

Introduction

The ability of electronic excited states to migrate through organic materials helps determine technological figures-of-merit like the "amplification" of fluorescence sensors[1−3] and the efficiency of photovoltaic cells.[4,5] Electronic energy transfer (EET) in an organic material is characterized by the diffusion constant D_{EET} and diffusion length L_D of the excited states or excitons. Because of its practical importance, a variety of experimental methods have been developed to measure the rate and spatial extent of EET in molecular systems. Polarization anisotropy experiments provide a way to measure the initial transfer step in a disordered medium.[6] But since these experiments are sensitive only to the initial EET event in orientationally disordered samples, they cannot provide a direct measure of L_D, which is determined by all of the subsequent hopping events.[7] Many workers have used an extrinsic dopant as a fluorescence quencher or acceptor.[8] By measuring the amount of host fluorescence quenching as a function of dopant concentration, such bulk quenching studies permit the determination of a diffusion length for the exciton in the host material. But in order to obtain quantitative information about L_D using the acceptor doping method, one must know the details of the host−acceptor EET interaction.[9] Furthermore, these experiments usually rest on the assumption that the presence of the acceptor molecule does not affect the properties of the host. While this may be the case in amorphous materials, it is likely that dopant molecules disrupt the packing of ordered host materials, for example, molecular crystals. Surface quenching of excitons at a second, spatially distinct layer avoids the issue of understanding the details of the host−guest interaction but leads to other problems.[10,11] In particular, this type of layered structure can have nontrivial optical properties, and phenomena like spatially nonuniform excitation and wave-guided host fluorescence can complicate the interpretation of the data.[8] Transient grating measurements provide a direct way to probe the spatial dependence of the EET without the introduction of a second chemical species into the host material.[12,13] But this nonlinear scattering experiment also requires a spatially homogeneous sample and high chromophore concentrations, while its spatial resolution is limited by the crossing angle of the laser beams. The different limitations of these techniques may provide an explanation for widely varying L_D values that currently exist in the literature for commonly studied materials like anthracene[8] and the polymer polyvinylcarbazole (PVK).[14,15]

The need for better tools to obtain reliable values for EET lengths has inspired the development of direct imaging techniques. Near-field scanning optical microscopy (NSOM) techniques have been used to directly image photobleaching patterns to deduce the exciton diffusion length in organic materials.[16,17] The chemical steps involved in photobleaching are not well-understood in most cases, however, and uncertainties about the roles of thermal transport and charged species may complicate the estimation of L_D. Direct spatial imaging of luminescence has been used to characterize self-absorption,[18] and Barbara and co-workers have shown that high-resolution diffraction-limited imaging of an NSOM excitation spot can provide a direct probe of the EET distance in organic materials.[19] One limitation of this approach is that it integrates the fluorescence image over

* Corresponding author. E-mail: christopher.bardeen@ucr.edu.

10.1021/jp072902t CCC: $37.00
Published on Web 08/02/2007

time. If one could time-resolve the image, one should be able to compare the early spot, unbroadened by diffusion, to later spots that exhibit broadening and thus directly measure the diffusive motion. Exciton diffusion in inorganic semiconductors has been studied using time-resolved pump−probe[20] and spatially resolved luminescence decays,[21,22] and recently, a Kerr gate microscope has been developed for picosecond time-resolved imaging of luminescence.[23] In this paper, we use the time-resolved projection of the emission spot onto the multichannel plate of a streak camera to obtain information about EET in molecular systems. By using this one-dimensional streak camera imaging (1D-SCI) experiment, we can directly visualize the spreading of a luminescence spot due to diffusive motion with picosecond resolution. We use the translational diffusion of excited-state platinum octaethylporphyrin as a proof-of-principle experiment. We then study EET in PVK, a material where recent experiments have suggested that L_D may be in the micron regime.[15] Preliminary experiments on disodium fluorescein, a molecule with a small fluorescence Stokes shift, result in anomalously rapid broadening, most likely due to fluorescence reabsorption and re-emission. We end by discussing possible improvements and limitations of the technique and estimate its ultimate utility for the study of EET in organic materials.

Experimental Section

Sample Preparation. Platinum octaethylporphyrin (PtOEP) was obtained from Frontier Scientific, Inc., and polymethylmethacrylate (PMMA), polyvinylcarbazole (PVK, M_w 1 100.000) and chlorobenzene (99.9%, HPLC grade) were obtained from Aldrich. Toluene (spectroscopic grade) is from EM Science; ethanol is from Gold Shield Chemical Co.; disodium fluorescein (DSF) is from Exciton; and Rhodamine 6G is from Lambda Physik. All chemicals were used as received. Dissolving 25.8 mg DSF in 2.5 mL basic ethanol (pH 13, made basic with KOH) gave 2.5×10^{-2} M solutions. Film samples were prepared by drop-casting PMMA/toluene or spin-casting PVK/chlorobenzene solutions on microscope slides. After drying, they were placed in an evacuated microscope cryostat (Janis ST-500), in order to avoid photooxidation and oxygen quenching. The concentration of PtOEP in PMMA was 5 μM (thickness of film = 0.9 μm), while that of PtOEP in toluene ranged from 5.5 μM to 650 μM, and PVK was used as a neat film with a thickness of 120 nm. Liquid samples were first degassed by bubbling argon through the solutions for 45 min, and then in a glovebox loaded into home-built 2.5 μm optical path length cuvettes, which consisted of two microscope slides sandwiched together with a 2.5 μm thick metal spacer and sealed with epoxy (Resin Formulators, RF-912). Samples were prepared with peak optical densities of less than 0.1 for the DSF and PtOEP samples and of less than 0.3 for the PVK films.

Photophysics. Steady-state UV−vis absorption and fluorescence data were taken using a Cary 50 Bio UV-visible spectrometer and a Spex Fluorolog Tau-3 fluorescence spectrophotometer (excitation at 400 nm), respectively.

The time-resolved fluorescence imaging data were obtained using either one-photon excitation at 400 nm (for PtOEP in toluene and PMMA) or two-photon excitation (for PVK and DSF) at 800 nm. The 800 nm pulses were generated by a 40 kHz regeneratively amplified Ti:sapphire laser system, while the 400 nm pulses were obtained by frequency doubling the amplified Ti:sapphire laser light (at an 8 kHz repetition rate) in a Type I BBO crystal. The pulse duration was 150−200 fs. The pulses were attenuated and directed into a home-built

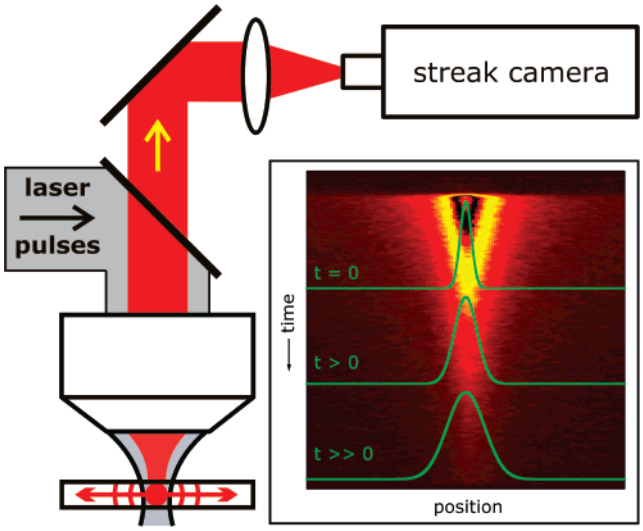

Figure 1. Schematic setup of the 1D-SCI experiment, which combines a far-field microscope with a picosecond time-resolved streak camera. The inset shows a streak camera image of an emission spot that broadens with time. The green lines illustrate schematically how the initially excited emission spot width disperses with time because of diffusion.

microscope with a 40 × 0.60 NA long working distance dry objective and a 500 mm tube lens, attached to a commercial picosecond streak camera (Hamamatsu C4334 Streakscope). The experimental setup is outlined in Figure 1. The magnification of the microscope was calibrated using a 130 lines/mm frequency target, which was illuminated from below, instead of the fluorescing sample, and determined to be 37.5, which corresponds to 29 pixels/μm on the streak camera. The fluorescence emission of all samples was collected by the microscope objective and directed back through a dichroic mirror to the tube lens and streak camera. Scattered excitation light was removed by placing filters (three hot mirrors for 800 nm excitation, two GG420 filters for 400 nm excitation) in front of the streak camera. Ambient light was kept from the detector by means of a light-tight enclosure around the instrument. For the PtOEP samples, approximately 5×10^8 laser shots were averaged over 3.5 h, while for PVK film samples 2×10^8 laser shots were averaged, all in photon-counting mode.

In order to realize a defined focal width using one-photon excitation of PtOEP molecules with 400 nm pulses, thin slabs (2.5 μm cuvette or <1 μm thin films) of PtOEP in toluene or PMMA were placed in the 400 nm focus. Direct imaging of the emission resulted in focal spots with full width at half-maximum (fwhm) diameters of 1.7 μm (800 nm pulses) and 1.4 μm (400 nm pulses, in toluene). Note that these spots are considerably larger than the theoretical diffraction limit of the objective lens, which is given by the resolution limit,[24]

$$\text{fwhm} = \frac{0.6\lambda}{\text{NA}} \tag{1}$$

where λ is the wavelength of light and NA is the numerical aperture of the lens. The relatively large spot sizes result from nonidealities in the focusing optics and the laser beam mode and from the fact that we did not overfill the lens aperture. The reason for not pushing the resolution limits of the microscope was to maintain reasonably well-behaved focal profiles that could be modeled in terms of easily analyzed Gaussian functions and to avoid the more complicated Airy functions which are associated with highly focused beams that overfill the back

aperture. The laser spot sizes and pulse energies resulted in maximum peak intensities of 5.0×10^9 W/cm^2 (800 nm pulses) and 1.6×10^9 W/cm^2 (400 nm pulses). The low laser intensities necessitated the long data acquisition times mentioned above but avoided artifacts like sample photobleaching and detector nonlinearity. In order to check the reproducibility of the data, we repeated the experiments for longer periods and also performed a pump power dependence study. In all of these cases, we saw no change in the results. Therefore, we conclude that PtOEP is photochemically stable at our experimental conditions.

To analyze the one-dimensional images obtained from the streak camera, we first assume that the emission spot is radially symmetric and can be represented by a weighted sum of Gaussian functions. In this case, the initial two-dimensional (2D) spot $I(x,y,0)$ is given by

$$I_{2D}(x,y,0) = A_1 \exp\left[-\frac{x^2+y^2}{{w_1}^2}\right] + A_2 \exp\left[-\frac{x^2+y^2}{{w_2}^2}\right] + \cdots \quad (2)$$

Note that an asymmetric excitation spot can be described by summing two off-center Gaussians without loss of generality. The time-evolution of this spot is then just given by the convolution of the initial distribution with a Gaussian broadening function:

$$I_{2D}(x,y,t) = I_{2D}(x,y,0) \otimes \mathrm{Diff}(x,y,t) \quad (3)$$

$$\mathrm{Diff}(x,y,t) = \frac{1}{\pi w_G(t)} \exp\left[-\frac{x^2+y^2}{{w_G}^2(t)}\right] \quad (4)$$

$w_G(t)$ is the adjustable parameter, which should be equal to $\sqrt{4Dt}$ for diffusive broadening. The convolution of these two functions results in

$$I_{2D}(x,y,t) = \frac{A_1}{\pi w_G(t)} \exp\left[-\frac{x^2+y^2}{{w_1}^2+{w_G}^2(t)}\right] + \frac{A_2}{\pi w_G(t)} \exp\left[-\frac{x^2+y^2}{{w_2}^2+{w_G}^2(t)}\right] + \cdots \quad (5)$$

In the 1D-SCI experiment, the two-dimensional diffusion is then mapped onto a one-dimensional multichannel plate, which effectively integrates over the y dimension:

$$I_{1D}(x,t) = \int_{-\infty}^{+\infty} \mathrm{d}y\, I_{2D}(x,y,t) \quad (6)$$

$$I_{1D}(x,t) = \frac{A_1'}{\sqrt{\pi w_G(t)}} \exp\left[-\frac{x^2}{{w_1}^2+{w_G}^2(t)}\right] + \frac{A_2'}{\sqrt{\pi w_G(t)}} \exp\left[-\frac{x^2}{{w_2}^2+{w_G}^2(t)}\right] + \cdots \quad (7)$$

Thus the 1D projection of the diffusion-broadened 2D profile is equivalent to convolving the initial 1D projection with a diffusion function. Rather than using a sum of Gaussians to describe the initial 1D profile of the excitation spot, we can use a different type of function which captures the shape of the one-dimensional profile, as long as it can be approximated by a sum of Gaussians. One such function is a Lorentzian profile with the width w_L.[25] In this case, the initial 1D projection is given by

$$I_{1D}(x,0) = \frac{w_L}{{w_L}^2 + 4x^2} \quad (8)$$

This function is then convolved with a 1D Gaussian broadening function with a 1/e half-width $w_G(t)$ in the same way as described above, and the formula used to describe the time-dependent 1D projection is

$$I_{1D}(x,t) = \frac{w_L}{{w_L}^2+4x^2} \otimes \frac{1}{w_G(t)\sqrt{\pi}} \exp\left[\frac{-x^2}{{w_G}^2(t)}\right] = \frac{w_L}{\sqrt{\pi}} \int_{-\infty}^{+\infty} \frac{\exp[-x'^2]}{{w_L}^2 + 4(x - w_G(t)x')^2}\,\mathrm{d}x' \quad (9)$$

One of the advantages of the time-resolved imaging approach is that it relies on measuring the relative changes in the spatial image and thus is not particularly sensitive to the initial shape of the excitation spot. In practice, the signal-to-noise ratio of the experiment will determine the amount of broadening that can be resolved and thus the smallest diffusive displacement that can be extracted from the data. In our experiments on PtOEP in toluene, for example, the Gaussian broadening parameter w_G has a standard deviation $\sigma_{wG} = 0.139$ μm, as compared with an initial 1/e half width of 0.829 μm. Thus, the uncertainty of the broadening divided by the initial width is 0.167 or ~17% detectable broadening within the error. For PtOEP in PMMA, where the signal-to-noise is better because of the longer luminescence lifetime, we obtain a ratio of 12%. In principle, these numbers could be improved by acquiring more data to increase the signal-to-noise and decrease the uncertainty in w_G. The experiments reported here required several hours of averaging; the ability to average for longer times is limited by the stability of the laser, the sample, or both.

Results and Discussion

In order to demonstrate the 1D-SCI method in a simple chemical system whose dynamics are well-understood, we first studied the phosphorescent dye PtOEP in room temperature toluene. The absorption and emission spectra of this molecule, shown in Figure 2a, are well-separated. The presence of the heavy metal atom in PtOEP results in a strongly allowed, long-lived phosphorescent emission centered at 645 nm. The lifetime of this emission has been measured to be 90−100 μs.[26,27] The phosphorescence decay time is 32 μs for a PtOEP sample in the 2.5 μm thick cell used in our experiments, as shown in Figure 2b. The shorter lifetime in our samples is probably due to the incomplete removal of residual O_2 in the glovebox atmosphere where the cells are filled and sealed. Thanks to the negligible overlap of the absorption and emission spectra, intermolecular energy transfer via resonant mechanisms (Förster transfer or radiative transfer via self-absorption) can be ruled out in this system. In toluene, the translational diffusion constant of PtOEP has been measured using NMR methods, which is found to be $D = 8.6 \times 10^{-6}$ cm^2/s.[27] Given this diffusion rate, the molecules can be expected to travel a distance

$$L_D = \sqrt{6D\tau_{ex}} = 406 \text{ nm} \quad (10)$$

within their excited-state lifetime $\tau_{ex} = 32$ μs. Thus, PtOEP provides a good test system for our 1D-SCI method: a long-lived excited-state gives rise to a measurable diffusion length,

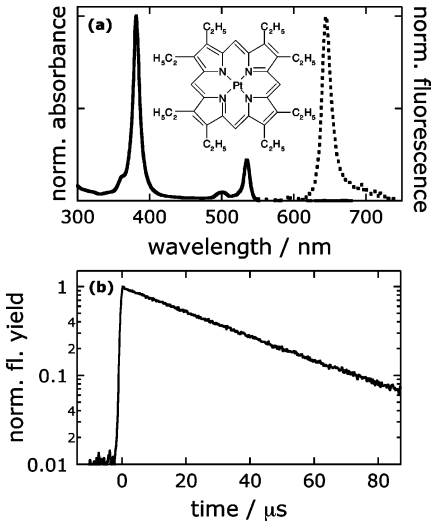

Figure 2. (a) Steady-state absorption (solid line) and phosphorescence (dashed line) spectra of PtOEP in toluene. The molecular structure of PtOEP is shown in the inset. (b) Phosphorescence decay of PtOEP in toluene solution in the 2.5 μm path length cell.

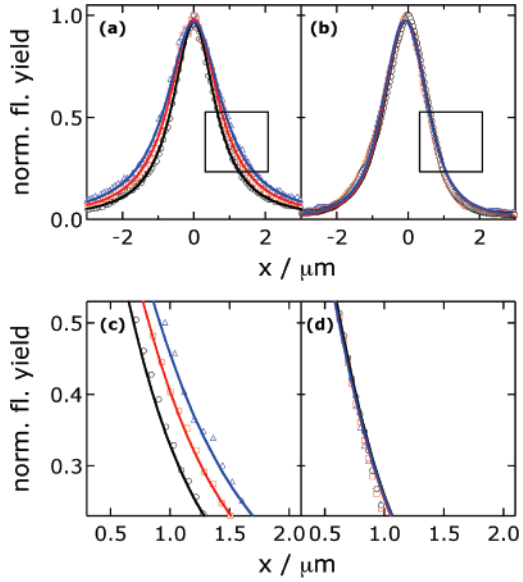

Figure 3. Spatial profiles of the emission spot as a function of time (integrated over 10 μs windows centered at 0 μs (black circles), 42 μs (red squares), and 84 μs (blue triangles); open symbols, data; solid lines, fits). (a) PtOEP in toluene shows broadening of the spot due to translational diffusion of the excited PtOEP molecules during their lifetime. (b) When PtOEP is embedded in the solid PMMA matrix, no broadening is observed. (c) and (d) Enlarged sections of the data and fits in (a) and (b), respectively.

while the mechanism of diffusion is straightforward and has been measured previously.

Figure 3a shows the results when the emission of PtOEP is projected onto the linear streak camera multichannel plate. The initial projection of the emission spot is well-approximated by a Lorentzian profile that broadens with time. There is a slight asymmetry in the initial spot, but we found that this had a negligible effect on the subsequent fits to the broadened profile. Even though the spot profile does not have an ideal Gaussian profile, as discussed in Experimental Section, the rate of broadening still provides information about the diffusion. The emission spot broadens with time, as expected because of the translational diffusion of the molecules outside of the laser focal spot. The broadened spots in Figure 3a are well-reproduced by convolving the initial Lorentzian profile with a Gaussian line

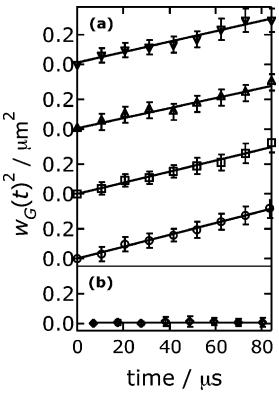

Figure 4. (a) Squared time-dependent half width at 1/e of the Gaussian part of the emission spot for four different concentrations of PtOEP in toluene. Circles: 650 μM, $D = (10.2 \pm 0.3) \times 10^{-6}$ cm^2/s. Squares: 320 μM, $D = (9.6 \pm 0.5) \times 10^{-6}$ cm^2/s. Up triangles: 64 μM, $D = (8.5 \pm 0.7) \times 10^{-6}$ cm^2/s. Down triangles: 5.5 μM, $D = (8.9 \pm 0.7) \times 10^{-6}$ cm^2/s. (b) Diffusive mean square displacement $w_G^2(t)$ of the emission spot of PtOEP in PMMA as a function of time. The solid lines are linear fits to the data.

shape with a time-dependent width. By fitting each 10 μs slice of the emission profile, we obtain a time-dependent Gaussian width $w_G(t)$, which is plotted in Figure 4 for various PtOEP concentrations. For all concentrations, the broadening increases linearly with time as expected for a diffusive process. From eq 5, the slope of the line allows us to obtain D. At the lowest concentration, 5.5×10^{-6} M, D is found to be $(8.9 \pm 0.7) \times 10^{-6}$ cm^2/s, which is identical to that obtained from NMR measurements to within the experimental error. At the highest concentration, D increases slightly to $(10.2 \pm 0.3) \times 10^{-6}$ cm^2/s. While the observed increase is close to the experimental error, it may reflect a slight enhancement of the energy diffusion rate at the highest concentrations due to intermolecular energy transfer. Such an effect has been shown to be significant for singlet−singlet energy transfer.[28−31] Triplet−triplet energy transfer arises from short-range interactions and requires close contact of the molecules, and its ability to enhance the apparent motion of the excited-state is expected to be much more limited. The collision rate k_{coll} for PtOEP in toluene can be calculated using the expression[27]

$$k_{coll} = 8\pi N_A D R_H C \qquad (11)$$

where N_A is Avogadro's number, D is the diffusion constant, $R_H = 0.5$ nm is the hydrodynamic radius for PtOEP, and C is the molar concentration. Using this expression, we find that an excited PtOEP molecule undergoes ~160 collisions with other PtOEP molecules in a 6.5×10^{-4} M solution during its 32 μs lifetime. Thus, there exist many opportunities for intermolecular energy transfer, although its effect on the overall energy diffusion appears to be quite small. In the dilute polymer solution, there is no chance for either translational or EET diffusion, and thus the time-dependent broadening is completely absent for a sample of PtOEP embedded in a solid polymer matrix. These experimental results are shown in Figure 3b,d. Note that in PMMA the PtOEP lifetime is 98 μs, which leads to greater signal levels at long delays and thus better signal-to-noise ratios in the beam profiles. A second point is that the initial spot has a Gaussian profile rather than a Lorentzian profile. This different profile is likely the result of weaker focusing of the laser beam in air (refractive index of 1.0) over the polymer sample as opposed to focusing through glass (refractive index of 1.5) into the toluene solution of PtOEP.

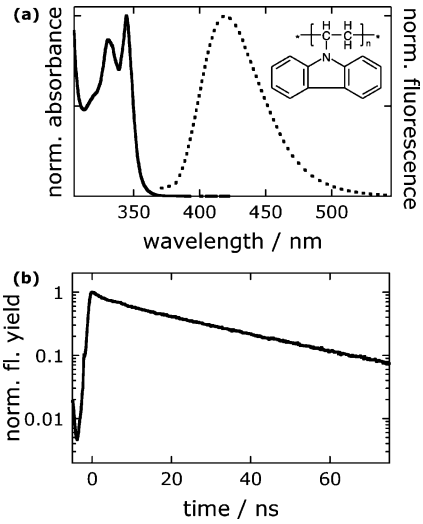

Figure 5. (a) Steady-state absorption (solid line) and fluorescence (dashed line) spectra, and (b) fluorescence decay of neat PVK film. The inset shows the molecular structure of PVK.

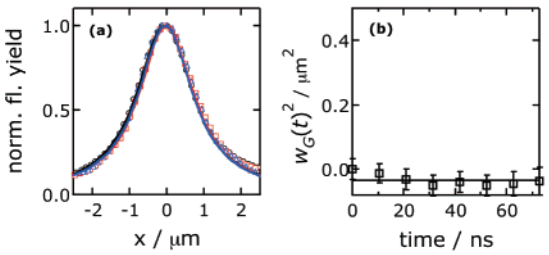

Figure 6. (a) Spatial profiles of the emission spot with time (integrated over 10 ns windows centered at 0 ns (black circles), 42 ns (red squares), and 73 ns (blue triangles); open symbols, data; solid lines, fits). (b) Diffusive mean square displacement $w_G^2(t)$ of the emission spot of neat PVK film as a function of time. The solid line is a linear fit to the data.

After using the PtOEP/toluene system to prove that the 1D-SCI technique can image the time-resolved diffusion of excited-state energy, we turned to a different molecular system where energy transfer occurs on a time scale of nanoseconds rather than microseconds. PVK is a polymer that is studied for its interesting electronic properties. The emission in PVK originates from excimers formed by separate carbazole units[14] and is shifted by at least 75 nm from the absorption edge, as seen from Figure 5a. The lifetime of the excimer luminescence seems to vary somewhat in the literature, with the 32 ns decay time of the excimer seen in our samples (Figure 5b) being somewhat longer than the 20 ns time commonly seen for the long-lived component in PVK.[32−34] Early work on energy transfer in PVK, in both isolated chains[35,36] and solid films,[14,37] resulted in estimates of the energy diffusion length ranging from 10 to 50 nm. Recently, experiments by Yu et al. using a layered donor−acceptor sample suggested that energy diffusion lengths in PVK could be much longer, on the order of 10 μm or greater.[15] We wanted to re-examine energy transfer in this system using the 1D-SCI technique, where such large lengths should be readily apparent. The results of these experiments are shown in Figures 6a,b. Note that the size of the excitation focus was slightly larger for this experiment than for the PtOEP experiments because of the use of two-photon excitation. As in the case of the PtOEP/PMMA data in Figure 3b, focusing through vacuum leads to a Gaussian initial profile rather than a Lorentzian. It is clear that there is no discernible broadening of the emission spot even up to delays of 60 ns. Our error bars suggest that a difference between w and w_0 down to the level of 200 nm should be detectable. This result is consistent with the earlier results on EET in PVK that estimate a diffusion length less than 100 nm.[14,37] The more recent results of Yu et al. may result from some process other than excimer-mediated energy transfer. Possible candidates include carrier diffusion and recombination or direct radiative transfer via fluorescence reabsorption.

The preliminary applications of the 1D-SCI method show that it is possible to use it to determine diffusion lengths as small as 150 nm. In its present realization, the experiment is limited by the relatively large excitation spot, which is a function of imperfections in the laser mode and our weak focusing conditions. The laser mode can be improved by spatial filtering. By increasing the input laser beam diameter by using a telescope and overfilling the rear aperture of the objective lens, we ought to be able to approach the diffraction-limited spot size, whose fwhm is given by eq 1. Given $\lambda = 400$ nm and an NA $= 0.6$ and assuming a focus in air, we get a minimum fwhm of the spot of 0.4 μm. If we are able to discern a 15% change in width, as described in Experimental Section, this suggests an ultimate resolution of the technique of 60 nm. Increasing the NA of the objective is another obvious approach to shrinking the spot size, but this is problematic for the following reasons. We want to study samples at different temperatures or that are air-sensitive. In the microscope cryostat used for our experiments, the sample is separated from the objective lens by a window at least 1 mm thick. The long working distances necessitated by this layer of glass preclude the use of very high NA objectives. Objectives with working distances greater than 1 mm are commercially available with NA's up to 0.8; so, in principle, we can ultimately gain up to a 30% improvement in resolution but at increased cost and decreased flexibility in the optical setup.

While a tighter focus provides greater resolution in the *xy* plane, it also decreases the Rayleigh range of the beam at the focus. A rapidly diverging beam leads to a blurring of the image spot and complicates the analysis of the broadening of the emission spot, since the point-spread function and optical transfer function of the imaging system would now have to be taken explicitly into account.[38] In the present work, we avoid this complication by using thin samples and laser beams that are not too highly focused so that the Rayleigh range of the focused beam is greater than the sample thickness. For a highly focused beam, this may not be possible. If the sample is made very thin, less than the exciton diffusion length, then surface effects may distort the diffusion dynamics through phenomena like surface quenching or trapping. One way to avoid beam divergence effects in a thick sample is to use multiphoton excitation, so that excitation occurs only inside the focal volume. As long as the fluorescence can escape the sample easily, this provides a way to simultaneously localize the focus and avoid possible surface quenching effects in a very thin sample.

A more fundamental problem with the 1D-SCI technique is one that also complicates other methods for the measurement of EET distances.[8] Radiative transfer due to reabsorption of the initially emitted luminescence has long been recognized as a mechanism that can distort the detected luminescence spectrum, decay dynamics, and spatial properties.[18,39−43] This phenomenon is expected to be most pronounced when there is significant overlap of the absorption and emission spectra. Unfortunately, this is also the situation where resonant mechanisms of EET, like Förster transfer, are expected to be most efficient. Distinguishing between these two phenomena in an imaging experiment can be difficult, especially since radiative energy transfer is a complicated process that depends sensitively on the geometrical properties of the initially excited region and the

sample. To look at this phenomenon, we performed preliminary experiments on concentrated (2.5×10^{-2} M) solutions of disodium fluorescein (DSF) in basic ethanol. DSF has a very small Stokes shift, resulting in a large overlap between absorption and fluorescence spectra. Using two-photon excitation in a 1 μm thick cell, the 1D-SCI experiment resolved a broadening of the emission spot on the nanosecond time scale that yielded an estimated $D = 5 \times 10^{-2}$ cm^2/s. This value is 2 orders of magnitude larger than the value of $\sim 10^{-4}$ cm^2/s obtained from transient grating measurements on similarly concentrated DSF solutions,[44] and also the value $D = 2.1 \times 10^{-4}$ cm^2/s obtained from measurements in our lab made using donor−acceptor transfer rates. In those experiments, we used varying concentrations of Rhodamine 6G as an acceptor and measured the change in the DSF fluorescence lifetime. We hypothesize that the discrepancy between the 1D-SCI measurements and the other two measurements is most likely due to radiative transfer between DSF molecules in the solution. In the simplest case, radiative transfer acts as a diffusive process with an effective diffusion constant D_{rad} given by[39,45−47]

$$D_{rad} \cong \frac{{l_{abs}}^2}{\tau_{ex}} \tag{12}$$

where l_{abs} is the penetration depth of a photon before reabsorption. The smallest value for l_{abs} (and thus the minimum radiative diffusion constant) is obtained from the path length of a photon at the peak of the DSF absorption, given by

$$l_{abs} = \frac{1}{\epsilon_{peak} C} \tag{13}$$

Using values for the peak absorption coefficient $\epsilon_{peak} = 92{,}300$ M^{-1} cm^{-1}[48] and a concentration $C = 2.5 \times 10^{-2}$ M, we obtain a value for $l_{abs} = 4.0$ μm. Given a $\tau_{ex} = 3.5$ ns as measured in our thin cell, we then obtain a $D_{rad} = 4.6 \times 10^{+1}$ cm^2/s. The measured D is 2 orders of magnitude smaller than this value. Thus, the value of D obtained from the 1D-SCI experiments is a factor of 100 too high to be explained by intermolecular Förster transfer and a factor of 100 too small to be explained by the simplest model of radiative transfer. Although the origin of this discrepancy is not clear, it is likely that the simplest model of radiative transport does not capture the full complexity of the process in our sample.[39] Clearly, more work is needed to determine the conditions where the 1D-SCI experiment can provide a reliable estimate of the nonradiative D_{EET} when there is significant overlap between the absorption and the emission spectra.

A final point is that our present analysis of the 1D-SCI images assumes that the energy diffusion is isotropic in all three dimensions. While this is likely to be the case for liquid or amorphous polymer systems, it is generally not the case for oriented systems like molecular crystals. Anisotropic EET in the *xy* plane would require a more advanced detection method. In these types of systems, either we would have to image the evolution of the entire spot using a two-dimensional detector or we would have to rotate the sample, taking one-dimensional cross sections of the spreading spot at regular intervals of rotation.

Conclusions

This paper has demonstrated the use of a new type of imaging experiment to directly look at the spatial motion of excited-state species in condensed phase systems. By coupling a streak camera to a far-field microscopy setup, we have demonstrated the ability to resolve broadening of the excitation spot that corresponds to diffusive displacements on the order of 150 nm. This experiment has been successfully used to image the translational diffusion of excited state PtOEP molecules in toluene solution, as well as the absence of long-range EET in the polymer PVK. By improving the spatial mode of the exciting laser beam and the focusing optics, it should be possible to attain a resolution of 60 nm using the 1D-SCI approach. Complications due to sample thickness, out-of-focus light, sample anisotropy, and radiative energy transfer have been discussed. This last phenomenon complicates the interpretation of any direct measurement of EET in systems where there is significant overlap of the absorption and emission spectra. Despite these challenges, the 1D-SCI method provides a new way to visualize EET in condensed phase systems and may prove useful in the study of organic semiconductors for solar cell applications, where the exciton diffusion length helps determine the photovoltaic efficiency.

Acknowledgment. We acknowledge the support of the National Science Foundation, Grant CHE-0517095. We thank Jeffery W. Lefler and Guido D. Frey for their technical support with the 2.5 μm cuvettes.

References and Notes

(1) Achyuthan, K. E.; Bergstedt, T. S.; Chen, L.; Jones, R. M.; Kumaraswamy, S.; Kushon, S. A.; Ley, K. D.; Lu, L.; McBranch, D.; Mukundan, H.; Rininsland, F.; Shi, X.; Xia, W.; Whitten, D. G. *J. Mater. Chem.* **2005**, *15*, 2648−2656.

(2) Fan, C.; Wang, S.; Hong, J. W.; Bazan, G. C.; Plaxco, K. W.; Heeger, A. J. *Proc. Natl. Acad. Sci. U.S.A.* **2003**, *100*, 6297−6301.

(3) McQuade, T. D.; Pullen, A. E.; Swager, T. M. *Chem. Rev.* **2000**, *100*, 2537−2574.

(4) Pettersson, L. A. A.; Roman, L. S.; Inganas, O. *J. Appl. Phys.* **1999**, *86*, 487−496.

(5) Peumans, P.; Yakimov, A.; Forrest, S. R. *J. Appl. Phys.* **2003**, *93*, 3693−3723.

(6) Gochanour, C. R.; Fayer, M. D. *J. Phys. Chem.* **1981**, *85*, 1989−1994.

(7) Gaab, K. M.; Bardeen, C. J. *J. Phys. Chem. A* **2004**, *108*, 10801−10806.

(8) Powell, R. C.; Soos, Z. G. *J. Lumin.* **1975**, *11*, 1−45.

(9) Soos, Z. G.; Powell, R. C. *Phys. Rev. B* **1972**, *6*, 4035−4046.

(10) Simpson, O. *Proc. R. Soc. London, Ser. A* **1957**, *238*, 402−411.

(11) Gregg, B. A.; Sprague, J.; Peterson, M. W. *J. Phys. Chem. B* **1997**, *101*, 5362−5369.

(12) Rose, T. S.; Righini, R.; Fayer, M. D. *Chem. Phys. Lett.* **1984**, *106*, 13−19.

(13) Eichler, H. J.; Gunter, P.; Pohl, D. W. *Laser-induced dynamic gratings*; Springer-Verlag: Berlin, Germany, 1986.

(14) Klopffer, W. *J. Chem. Phys.* **1969**, *50*, 2337−2343.

(15) Yu, J. W.; Kim, J. K.; Cho, H. N.; Kim, D. Y.; Kim, C. Y.; Song, N. W.; Kim, D. *Macromolecules* **2000**, *33*, 5443−5447.

(16) Higgins, D. A.; Barbara, P. F. *J. Phys. Chem.* **1995**, *99*, 3−7.

(17) Credo, G. M.; Lowman, G. M.; DeAro, J. A.; Carson, P. J.; Winn, D. L.; Buratto, S. K. *J. Chem. Phys.* **2000**, *112*, 7864−7872.

(18) Freeark, C. W.; Hardwick, R. *J. Chem. Phys.* **1959**, *63*, 194−198.

(19) Adams, D. M.; Kerimo, J.; O'Connor, D. B.; Barbara, P. F. *J. Phys. Chem. A* **1999**, *103*, 10138−10143.

(20) Smith, L. M.; Wake, D. R.; Wolfe, J. P.; Levi, D.; Klein, M. V.; Klem, J.; Henderson, T.; Morkoc, H. *Phys. Rev. B* **1988**, *38*, 5788−5791.

(21) Heller, W.; Filoramo, A.; Roussignol, P.; Bockelmann, U. *Solid-State Electron.* **1996**, *40*, 725−728.

(22) Hagn, M.; Zrenner, A.; Bohm, G.; Weimann, G. *Appl. Phys. Lett.* **1995**, *67*, 232−234.

(23) Fujino, T.; Fujima, T.; Tahara, T. *Appl. Phys. Lett.* **2005**, *87*, 131105/1−131105/3.

(24) Lipson, S. G.; Lipson, H. *Optical Physics*, 2nd ed.; Cambridge University Press: Cambridge, U.K., 1981.

(25) Douglass, D. C.; Peterson, G. E.; McBrierty, V. J. *Phys. Rev. B* **1989**, *40*, 10694−10703.

(26) Pan, S.; Rothberg, L. J. *J. Am. Chem. Soc.* **2005**, *127*, 6087−6094.

(27) Yang, J.; Cyr, P. W.; Wang, Y.; Soong, R.; Macdonald, P. M.; Chen, L.; Manners, I.; Winnik, M. A. *Photochem. Photobiol.* **2006**, *82*, 262−267.

(28) Pandey, K. K.; Pant, T. C. *Chem. Phys. Lett.* **1990**, *170*, 244−252.

(29) Joshi, H. C.; Mishra, H.; Tripathi, H. B.; Pant, T. C. *J. Lumin.* **2000**, *90*, 17−25.

(30) Gosele, U.; Hauser, M.; Klein, U. K. A.; Frey, R. *Chem. Phys. Lett.* **1975**, *34*, 519−522.

(31) Jang, S.; Shin, K. J.; Lee, S. *J. Chem. Phys.* **1995**, *102*, 815−827.

(32) Venikouas, G. E.; Powell, R. C. *Chem. Phys. Lett.* **1975**, *34*, 601−604.

(33) Peter, G.; Bassler, H.; Schrof, W.; Port, H. *Chem. Phys.* **1985**, *94*, 445−453.

(34) Byun, H. Y.; Chung, I. J.; Shim, H. K.; Kim, C. Y. *Chem. Phys. Lett.* **2004**, *393*, 197−203.

(35) Webber, S. E.; Avots-Avotins, P. E.; Deumie, M. *Macromolecules* **1981**, *14*, 105−110.

(36) Rauscher, U.; Bassler, H. *Macromolecules* **1990**, *23*, 398−405.

(37) Powell, R. C.; Kim, Q. *J. Lumin.* **1973**, *6*, 351−361.

(38) Gu, M. *Advanced Optical Imaging Theory*; Springer: New York, 1999.

(39) Molisch, A. F.; Oehry, B. P. *Radiation trapping in atomic vapours*; Oxford University Press: Oxford, U.K., 1998.

(40) Berberan-Santos, M. N.; Pereira, E.; Martinho, J. M. G. In *Resonance Energy Transfer*; Andrews, D. L., Demidov, A. A., Eds.; John Wiley and Sons: Chichester, U.K., 1999.

(41) Pereira, E. J. N.; Berberan-Santos, M. N.; Fedorov, A.; Vincent, M.; Gallay, J.; Martinho, J. M. G. *J. Chem. Phys.* **1999**, *110*, 1600−1610.

(42) Hammond, P. R. *J. Chem. Phys.* **1979**, *70*, 3884−3894.

(43) Birks, J. B. *Photophysics of aromatic molecules*; Wiley & Sons: London, 1970.

(44) Gomez-Jahn, L.; Kasinski, J.; Miller, R. J. D. *Chem. Phys. Lett.* **1986**, *125*, 500−506.

(45) Milne, E. A. *J. London Math. Soc.* **1926**, *1*, 40−51.

(46) Holstein, T. *Phys. Rev.* **1947**, *72*, 1212−1233.

(47) Blickensderfer, R. P.; Breckenridge, W. H.; Simons, J. *J. Phys. Chem.* **1976**, *80*, 653−659.

(48) Seybold, P. G.; Gouterman, M.; Callis, J. *Photochem. Photobiol.* **1969**, *9*, 229−242.